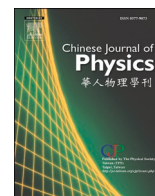




ELSEVIER

Contents lists available at ScienceDirect

Chinese Journal of Physics

journal homepage: [www.sciencedirect.com/journal/chinese-journal-of-physics](http://www.sciencedirect.com/journal/chinese-journal-of-physics)

# MHD flow and heat transfer of a hybrid nanofluid past a nonlinear surface stretching/shrinking with effects of thermal radiation and suction

A'isyah Jaafar<sup>a</sup>, Iskandar Waini<sup>b</sup>, Anuar Jamaludin<sup>a,\*</sup>, Roslinda Nazar<sup>c</sup>, Ioan Pop<sup>d</sup>

<sup>a</sup> Department of Mathematics, Universiti Pertahanan Nasional Malaysia, 57000 Kuala Lumpur, Malaysia

<sup>b</sup> Fakulti Teknologi Kejuruteraan Mekanikal dan Pembuatan, Universiti Teknikal Malaysia Melaka, Hang Tuah Jaya, 76100 Durian Tunggal, Melaka, Malaysia

<sup>c</sup> Department of Mathematical Sciences, Faculty of Science and Technology, Universiti Kebangsaan Malaysia, 43600, Bangi, Selangor, Malaysia

<sup>d</sup> Department of Mathematics, Babeş-Bolyai University, R-400084 Cluj-Napoca, Romania

## ARTICLE INFO

### Keywords:

Dual solution  
Hybrid nanofluid  
Magnetohydrodynamics  
Stability analysis  
Thermal radiation

## ABSTRACT

The essence of this study is to explore the nonlinearly stretching/shrinking hybrid nanofluid in terms of its steady flow and heat transfer with the effects of magnetohydrodynamics (MHD), thermal radiation, and suction. The governing partial differential equations are modified by similarity solution into nonlinear ordinary differential equations and solved numerically by *bvp4c*. The effects of profile on both velocity and temperature, the skin friction coefficient, and the Nusselt number were examined. It was discovered that dual solutions were present, and water has superior heat transfer performance compared to nanofluids and hybrid nanofluids. The thermal boundary layer thickness increases as magnetic and suction parameters increase. According to the stability analysis, first solution is steady, and second solution is unsteady.

## 1. Introduction

Nanofluid is a colloidal composition of nanoparticles ranging from 1 to 100 nm and a base liquid. The selection of the base fluid-particle combination is dependant on the intended use of the nanofluid. The nanoparticles include metals (Al, Cu, Si, K, Ni, Ag), metal carbide (SiC), metal oxides (Al<sub>2</sub>O<sub>3</sub>, CuO, MgO, ZnO, Fe<sub>2</sub>O<sub>3</sub>, TiO<sub>2</sub>), carbon materials (CNTs, MWCTNs, diamond, graphite) and metal nitride (AlN). The nanoparticle later was mixed with base liquid such as water, ethylene glycol, transformer oil, paraffin oil, naphthenic mineral oil, and vegetable oil to create nanofluid. According to previous research, nanofluids exhibit thermophysical properties that are twice as high as those of conventional fluids, even when only small percentage is involved in fluid flow. This potential leads to the application of nanofluid in engineering, sciences, industrial sectors, and industrial geometries. Moreover, [1] added that nanofluid practically used in technological such as coolants in transformers, cars, computers and machines. Recently, the studies of nanofluid was expanded in numerous fields such as thin needle by [2], rotating disk by [3], magnetohydrodynamics (MHD) by [4], porous media by [5], nonlinear thermal radiation by [6,7], viscous dissipation by [8], heat generation by [9,10].

Hybrid nanofluids are the further improvement in thermal conductivity that can be achieved by hybridization of various nanoparticles. The examples of two different nanoparticles mixture under a base liquid (water) are Silver-Silicon (Ag/Si), Silver-Magnesium

\* Corresponding author.

E-mail address: [mohdanuar@upnm.edu.my](mailto:mohdanuar@upnm.edu.my) (A. Jamaludin).

<https://doi.org/10.1016/j.cjph.2022.06.026>

Received 26 April 2022; Received in revised form 21 June 2022; Accepted 29 June 2022

Available online 1 July 2022

0577-9073/© 2022 The Physical Society of the Republic of China (Taiwan). Published by Elsevier B.V. All rights reserved.

Oxide (Ag/MgO), Copper-Alumina ( $\text{Al}_2\text{O}_3/\text{Cu}$ ), Copper-Titanium Dioxide ( $\text{TiO}_2/\text{Cu}$ ) and Silicon Carbide-Titanium Dioxide ( $\text{TiO}_2/\text{SiC}$ ). [11] reported that there several techniques in hybridising mixture of nanoparticle such as two-step technique, ball milling, in-situ, chemical reduction, chemical vapour deposition, mechanical alloying, wet chemical and solve thermal. He added, researchers utilise the two-step process most frequently due to its low cost and capacity to generate hybrid nanofluids on a big scale. The motive for using hybrid nanofluid is to further optimize the thermal exchange between the properties and drawbacks of individual suspensions due to their perfect proportion rate and thermal system. The frequently applied hybrid nanoparticles by researchers are  $\text{Al}_2\text{O}_3/\text{Cu}$  since the composites have excellent electrical conductivity, thermal conductivity, and arc erosion resistance. The application of hybrid nanofluid are automotive cooling, generator cooling, nuclear system coolant, electro-mechanical, and renewable energy. Recent years have witnessed an expansion of nanofluid research in several sectors such as mixed convection by [12,13], porous media by [14], Joule heating by [15], stagnation point by [16,17], mass transpiration by [18], suction by [19] and Marangoni convective by [20].

The flow caused by stretching sheet is a crucial factor in fluid mechanics due to its involvement in real-world situation. The extensive application of stretching sheet is various in the industry including polymer sheet extractors, micro fluidics, wire drafting, transportation, and paper development. [21] reported that stretching sheet important in the field of metal extrusion, manufacturing, space acoustics glass blowing and avionics. Even though most of the literature focuses on analysing boundary layer flow with a linear surface, stretching is not necessarily linear, and few authors have investigated nonlinear stretching sheets. The studies of stretching sheet have been reported in [22–25], the exponentially stretching sheet in [9], the stretching curve sheet in [26], the stretching cylinder in [27] and the stretching/shrinking problems in [28–34].

MHD has recently gained recognition as the quality of its applications has increased, particularly in astrophysics, medicine, optical transplantation, resonator fibre optic filtering, recrystallization, metal extrusion, environmental chemical technology, geophysical sciences, and petroleum engineering. MHD is achieved by generating a magnetic field orthogonal to the direction of the fluid flow, which may produce an induced drag known as the Lorentz force. The magnetic field functions by extending the boundary layer's dispersion, decreasing fluid motion, and increasing fluid concentration and temperature. The reaction of MHD were examined in [35, 36] with effects of heat source/sink, [37–39] with thermal radiation, [40] with viscous dissipation, [41] with Joule heating, [42] with mixed convection and [43] with stagnation point. Additionally, the effects of MHD were reported by [44] under micro channel, [45] under rotating disk, [24,46] under non-Newtonian fluid flow, [47] under Casson fluid flow, [48,49] under micropolar fluid flow, [50] under ferrofluid flow and [51] under hybrid ferrofluid flow.

At high operating temperatures, the influence of thermal radiation on heat transfer rate and temperature profiles can be pretty remarkable. Therefore, the number of studies on thermal radiation effects under the boundary layer problems is expanding. Thermal radiation has helped develop improved energy conversion systems designed to operate at elevated temperatures. The study of Casson fluid reported by [23] stated that thermal radiation and nonlinear thermal radiation are utilised in numerous fields, including spacecraft, paper and glass production, gas turbines, space technology, and hypersonic flight. The researchers who have investigated the thermal radiation are [7] involving activation energy, [37–39] involving MHD, and [52] involving Joule heating, [53] involving heat source/sink, and [54] involving interfacial layer and shape effects.

Suction is a technique for managing boundary layers of external flows to decrease friction and energy losses across pipelines. It should be implemented on surfaces, pores, holes, perforations, apertures, or permeable components. These holes are frequently used to erode the boundary layer proximity to the wall slowly. As a response, the velocity profile of the boundary layer becomes more overfilled, thus more stable in terms of separation. Due to these advantages, several researchers investigated the effect of suction on hybrid nanofluids in [55–58], while [59] on rotating sphere.

The development of hybrid nanofluids has been reported by researchers in the past years, but the studies of nonlinearly stretching and shrinking surfaces under hybrid nanofluid flow are still insufficient. As a result, the goal of this research is to fill in the significant advancement of hybrid nanofluid under the influences of MHD, thermal radiation, and suction, specifically under nonlinearly stretching/shrinking surfaces. The changes in thermal radiation and suction behaviour were also to be observe as MHD was applied. The mathematical modelling for the MHD flow and heat transfer on a hybrid nanofluid will be investigated in this research. The analysis will be conducted using mathematical models based on the Tiwari and Das model [60]. Motivated by the [31] studies, the study investigates nonlinearly stretching/shrinking sheets with magnetic, radiation, and suction parameters. The partial differential equations (PDE) models were modified into ordinary differential equations (ODE) with similarity transformations. Numerical solutions of the simplified equations will then be performed using MATLAB's bvp4c program. Additionally, the occurrence of dual solutions will be investigated as well. As a result, dual solutions stability will be determined using the [61] initiated stability analysis. It is vital to construct a strategy for establishing the stability of dual solutions because it establishes a procedure for determining which solution is stable. This research aims to examine the effect of controlling parameters on hybrid nanofluid's flow and heat transfer properties. The skin friction coefficient, the velocity profile, the local Nusselt number, and the temperature profiles will be tabulated and analysed for various controlling parameter and copper nanoparticle volume fraction.

## 2. Mathematical formulation

Considering a continuous two-dimensional magnetohydrodynamic (MHD) flow and heat transfer involving thermal radiation and suction across a nonlinearly stretching/shrinking surface on a hybrid nanofluid. The mixture of Cu and  $\text{Al}_2\text{O}_3$  in a base fluid, water, was chosen as the type of hybrid nanofluid. The Cu metal nanoparticles exhibit a rapid rate of heat transfer and surface shear stress while the  $\text{Al}_2\text{O}_3$  nanoparticles are utilised due to their chemical immobility and stability. Thus, the hybrid nanofluid has the capability of improving the stability and thermophysical characteristics. The setting is on an accelerating stretching or shrinking surface with an additional magnetic field while the flow of hybrid nanofluid is steady and incompressible. A parallel x-and y-axis coordinate frame is

measured following Cartesian coordinates of the plate at  $y = 0$ . The governing equations in (1)–(3) consist of the continuity equation, momentum equation, and energy equation, respectively. The MHD was positioned in the momentum equation while thermal radiation was positioned in the energy equation. The boundary conditions in (4) are required to verify the physical and time-dependant boundary conditions of the medium. The stretching or shrinking surface ( $u_w(x)$ ) and the mass flux ( $v_w(x)$ ) are assumingly positioned with velocity. Meanwhile, the surface temperature ( $T_w$ ) and far-field fluid temperature ( $T_\infty$ ) are presumed to be constant. Furthermore, the shape and nanostructures of hybrid nanofluids are uniform and homogenous, and the effects of aggregation are not considered because the nanofluids are made up of a constant mixture.

The hybrid nanofluid governing equations for fluid flow and heat transfer models are as follows [21,31,60]:

$$\frac{\partial u}{\partial x} + \frac{\partial v}{\partial y} = 0, \tag{1}$$

$$u \frac{\partial u}{\partial x} + v \frac{\partial u}{\partial y} = \frac{\mu_{hnf}}{\rho_{hnf}} \frac{\partial^2 u}{\partial y^2} - \frac{\sigma_{hnf} B^2}{\rho_{hnf}} u, \tag{2}$$

$$u \frac{\partial T}{\partial x} + v \frac{\partial T}{\partial y} = \alpha_{hnf} \frac{\partial^2 T}{\partial y^2} - \frac{1}{(\rho C_p)_{hnf}} \frac{\partial q_r}{\partial y}, \tag{3}$$

focusing on the boundary conditions:

$$\begin{aligned} u &= cu_w(x), v = v_w(x), T = T_w, \text{ at } y = 0, \\ u &\rightarrow 0, T \rightarrow T_\infty, \text{ as } y \rightarrow \infty, \end{aligned} \tag{4}$$

where  $u$  and  $v$  signify the velocity elements in the  $x$ - and  $y$ -axes, sequentially. Moreover,  $B$  denotes the uniform magnetic field, the temperature of hybrid nanofluid is denoted by  $T$ , and  $c$  signifies regular stretching ( $c > 0$ ), shrinking ( $c < 0$ ), or static ( $c = 0$ ). In addition,  $q_r$  is the radiative heat transfer rate. The radiative heat flow is readily stated as follows using Roselland’s approximation:

$$q_r = -\frac{4}{3} \frac{\sigma}{k^*} \frac{\partial T^4}{\partial y}, \tag{5}$$

in which  $k^*$  is the mean absorption coefficient while Stefan-Boltzmann constant is denoted as  $\sigma$ . Eq. (6) is obtained using  $T^4 \approx 4T_\infty^3 T - 3T_\infty^4$ , which are the result of extending  $T^4$  utilizing a Taylor series about  $T_\infty$  and ignoring the terms of higher-order. Following that, the equation of energy in (3) becomes as follows:

$$u \frac{\partial T}{\partial x} + v \frac{\partial T}{\partial y} = \alpha_{hnf} \frac{\partial^2 T}{\partial y^2} + \frac{16\sigma T_\infty^3}{3(\rho C_p)_{hnf} k^*} \frac{\partial^2 T}{\partial y^2}. \tag{6}$$

Additionally,  $\mu_{hnf}$  denotes the hybrid nanofluid’s dynamic viscosity,  $\rho_{hnf}$  denotes the hybrid nanofluid’s density,  $\sigma_{hnf}$  denotes the hybrid nanofluid’s electrical conductivity, and  $\alpha_{hnf} = k_{hnf}/(\rho C_p)_{hnf}$  denotes the hybrid nanofluid’s thermal diffusivity, where  $k_{hnf}$  is the hybrid nanofluid’s thermal conductivity and  $(\rho C_p)_{hnf}$  is the hybrid nanofluid’s heat capacitance. Tables 1 and 2 illustrate the mathematical frameworks for the thermophysical attributes of the nanofluid and hybrid nanofluid, correspondingly.

To derive similarity solutions of the hybrid nanofluid’s governing Eqs. (1),(2), and (6) subject to (4), the terms  $B(x)$ ,  $u_w(x)$  and  $v_w(x)$  are expressed as follows:

$$B(x) = B_0 \nu_f^{1/2} x^{-1/3} L^{-2/3}, \quad u_w(x) = \nu_f x^{1/3} L^{-4/3}, \quad v_w(x) = -\frac{2}{3} \nu_f x^{-1/3} L^{-2/3} s, \tag{7}$$

where  $B_0$  is a constant,  $\nu_f$  is the base fluid kinematic viscosity,  $L$  is the characteristic length of the surface, and  $s$  is the suction/injection parameter.

Next, the following similarity factors are utilized, as suggested by [62]:

**Table 1**  
The base fluid and nanoparticle thermophysical characteristics.

Property	Water (base fluid at 25°C)	Cu	Al <sub>2</sub> O <sub>3</sub>
$C_p$ (J/kgK)	4179	385	765
$k$ (W/mK)	0.613	400	40
$\rho$ (kg/m <sup>3</sup> )	997.1	8933	3970
$\sigma$ (s/m)	$5.5 \times 10^{-6}$	$59.6 \times 10^6$	$35 \times 10^6$
Prandtl number (Pr)	6.2	–	–

**Table 2**  
The nanofluid and hybrid nanofluid thermophysical characteristics.

Properties	Nanofluids
Density	$\rho_{nf} = (1 - \phi_1)\rho_f + \phi_1\rho_{s1}$
Heat capacity	$(\rho C_p)_{nf} = (1 - \phi_1)(\rho C_p)_f + \phi_1(\rho C_p)_{s1}$
Dynamic viscosity	$\mu_{nf} = \frac{\mu_f}{(1 - \phi_1)^{2.5}}$
Electrical conductivity	$\frac{\sigma_{nf}}{\sigma_f} = 1 + \frac{3(\sigma_{s1}/\sigma_f - 1)\phi_1}{\sigma_{s1}/\sigma_f + 2 - (\sigma_{s1}/\sigma_f - 1)\phi_1}$
Thermal conductivity	$k_{nf} = \frac{k_{s1} + 2k_f - 2\phi_1(k_f - k_{s1})}{k_{s1} + 2k_f + \phi_1(k_f - k_{s1})} \times (k_{nf})$
Properties	Hybrid Nanofluids
Density	$\rho_{hnf} = (1 - \phi_2)[(1 - \phi_1)\rho_f + \phi_1\rho_{s1}] + \phi_2\rho_{s2}$
Heat capacity	$(\rho C_p)_{hnf} = (1 - \phi_2)[(1 - \phi_1)(\rho C_p)_f + \phi_1(\rho C_p)_{s1}] + \phi_2(\rho C_p)_{s2}$
Dynamic viscosity	$\mu_{hnf} = \frac{\mu_f}{(1 - \phi_1)^{2.5}(1 - \phi_2)^{2.5}}$
Electrical conductivity	$\frac{\sigma_{hnf}}{\sigma_{bf}} = \frac{\sigma_{s2} + 2\sigma_{bf} - 2\phi_2(\sigma_{bf} - \sigma_{s2})}{\sigma_{s2} + 2\sigma_{bf} + \phi_2(\sigma_{bf} - \sigma_{s2})}$ where $\frac{\sigma_{bf}}{\sigma_f} = \frac{\sigma_{s1} + 2\sigma_f - 2\phi_1(\sigma_f - \sigma_{s1})}{\sigma_{s1} + 2\sigma_f + \phi_1(\sigma_f - \sigma_{s1})}$
Thermal conductivity	$k_{hnf} = \frac{k_{s2} + 2k_{nf} - 2\phi_2(k_{nf} - k_{s2})}{k_{s2} + 2k_{nf} + \phi_2(k_{nf} - k_{s2})} \times (k_{nf})$

$$\begin{aligned}
 (a) \quad u &= \nu_f x^{1/3} L^{-4/3} f'(\eta), \\
 (b) \quad v &= -\frac{1}{3} \nu_f x^{-1/3} L^{-2/3} (2f(\eta) - \eta f'(\eta)), \\
 (c) \quad \theta(\eta) &= \frac{T - T_\infty}{T_w - T_\infty}, \\
 (d) \quad \eta &= x^{-1/3} L^{-2/3} y,
 \end{aligned}
 \tag{8}$$

where ' denotes distinction from  $\eta$ . By introducing the following similarity variables (8) into Eqs. (2) and (6), the corresponding similarity equations are generated:

$$3 \frac{\mu_{hnf} f'''}{\mu_f} + \frac{\rho_{hnf}}{\rho_f} (2ff'' - f'^2) - 3 \frac{\sigma_{hnf}}{\sigma_f} M f' = 0,
 \tag{9}$$

$$\frac{3}{Pr} \left[ \frac{k_{hnf}}{k_f} + \frac{4}{3} R \right] \theta'' + 2 \frac{(\rho C_p)_{hnf}}{(\rho C_p)_f} f \theta' = 0,
 \tag{10}$$

whereas the boundary conditions (4) now have the following form:

$$\begin{aligned}
 f(0) &= s, \quad f'(0) = c, \quad \theta(0) = 1, \\
 f'(\eta) &= 0, \quad \theta(\eta) = 0 \quad \text{as} \quad \eta \rightarrow \infty.
 \end{aligned}
 \tag{11}$$

Note that  $M$  denotes the parameter of magnetic,  $Pr$  refers to the number of Prandtl and  $R$  is the parameter of radiation, which are defined as written below:

$$M = \frac{\sigma_f B_0^2}{\rho_f}, \quad Pr = \frac{\mu_f (C_p)_f}{k_f}, \quad R = \frac{4\sigma T_\infty^3}{k^* k_f}.
 \tag{12}$$

The skin friction coefficient  $C_f$  and the local Nusselt number  $Nu_x$  are the physical factors of practical significance, defined as follows:

$$C_f = \frac{\tau_w}{\rho_f u_w^2}, \quad Nu_x = \frac{xq_w}{k_f(T_w - T_\infty)},
 \tag{13}$$

where  $\tau_w$  denotes the wall shear stress and  $q_w$  denotes the surface heat flux, as stated below:

$$\tau_w = \mu_{hnf} \left( \frac{\partial u}{\partial y} \right)_{y=0}, \quad q_w = -k_{hnf} \left( \frac{\partial T}{\partial y} \right)_{y=0} + (q_r)_{y=0}.
 \tag{14}$$

Substituting Eq. (8) into Eqs. (13) and (14) yields

$$\text{Re}_x^{1/2} C_f = \frac{\mu_{hnf}}{\mu_f} f''(0), \text{Re}_x^{-1/2} Nu_x = - \left[ \frac{k_{hnf}}{k_f} + \frac{4}{3} R \right] \theta'(0), \tag{15}$$

where the Reynolds number at the local level  $\text{Re}_x$  is denoted by

$$\text{Re}_x = \frac{u_w(x)x}{\nu_f}. \tag{16}$$

The thermophysical attributes of water and nanoparticles are shown in Table 1, while those of nanofluid and hybrid nanofluid are shown in Table 2. Both are sources from [31] and [63]. Note that  $\rho_f$  and  $\rho_s$  are the densities of water and hybrid nanoparticles, respectively. The nanoparticle volume fraction of aluminium oxide ( $\text{Al}_2\text{O}_3$ ) and copper (Cu) are referred to the symbols of  $\phi_1$  and  $\phi_2$ , respectively. Next, the thermal conduction of the water and the hybrid nanoparticles are denoted by  $k_f$  and  $k_s$ , proportionately. The heat capacity of constant pressure is denoted by  $C_p$ . Meanwhile,  $(\rho C_p)_f$  and  $(\rho C_p)_s$  are referred to as the heat capacitance of water and hybrid nanoparticles sequentially.

### 3. Stability analysis

The dual solution’s stability to the boundary value problem Eqs. (9) – (11) was investigated using temporal stability analysis. Stability analysis in [34,61,64] were deployed to show that the boundary value problem has dual solutions. Following [61], the developed new dimensionless time variable  $\tau$  related to an initial value problem corresponding to the concern over what solution would be attained in actuality. As a result, we have:

$$\frac{\partial u}{\partial t} + u \frac{\partial u}{\partial x} + v \frac{\partial u}{\partial y} = \frac{\mu_{hnf}}{\rho_{hnf}} \frac{\partial^2 u}{\partial y^2} - \frac{\sigma_{hnf} B^2}{\rho_{hnf}} u, \tag{17}$$

$$\frac{\partial T}{\partial t} + u \frac{\partial T}{\partial x} + v \frac{\partial T}{\partial y} = \alpha_{hnf} \frac{\partial^2 T}{\partial y^2} + \frac{16\sigma T_\infty^3}{3(\rho C_p)_{hnf} k^*} \frac{\partial^2 T}{\partial y^2}, \tag{18}$$

where  $t$  signifies the flow of time, where the accompanying new similarity transformation was produced in conjunction with the similarity equations in (8), given by

$$\begin{aligned} (a) \quad u &= \nu_f x^{1/3} L^{-4/3} \frac{\partial f}{\partial \eta}, \\ (b) \quad v &= -\frac{1}{3} \nu_f x^{-1/3} L^{-2/3} \left[ 2f - \eta \frac{\partial f}{\partial \eta} - 2\tau \frac{\partial f}{\partial \tau} \right], \\ (c) \quad \theta(\eta, \tau) &= \frac{T - T_\infty}{T_w - T_\infty}, \\ (d) \quad \eta &= x^{-1/3} L^{-2/3} y, \\ (e) \quad \tau &= \frac{1}{3} \nu_f x^{-2/3} L^{-4/3} t. \end{aligned} \tag{19}$$

Thus, Eqs. (17) and (18) were expressed in the following form

$$3 \frac{\mu_{hnf}}{\mu_f} \frac{\partial^3 f}{\partial \eta^3} + \frac{\rho_{hnf}}{\rho_f} \left( 2f \frac{\partial^2 f}{\partial \eta^2} - \frac{\partial^2 f}{\partial \eta \partial \tau} - \left( \frac{\partial f}{\partial \eta} \right)^2 \right) - 3M \frac{\sigma_{hnf}}{\sigma_f} \frac{\partial f}{\partial \eta} = 0, \tag{20}$$

$$\frac{3}{\text{Pr}} \left( \frac{k_{hnf}}{k_f} + \frac{4}{3} R \right) \frac{\partial^2 \theta}{\partial \eta^2} - \frac{(\rho C_p)_{hnf}}{(\rho C_p)_f} \frac{\partial \theta}{\partial \tau} + 2f \frac{(\rho C_p)_{hnf}}{(\rho C_p)_f} \frac{\partial \theta}{\partial \eta} = 0. \tag{21}$$

The boundary conditions, on the other hand, may be written as follows:

$$\begin{aligned} f(\eta, \tau) = s, \quad \frac{\partial f}{\partial \eta}(\eta, \tau) = c, \quad \theta(\eta, \tau) = 1 \quad \text{at} \quad \eta = 0, \\ \frac{\partial f}{\partial \eta}(\eta, \tau) = 0, \quad \theta(\eta, \tau) = 0 \quad \text{as} \quad \eta \rightarrow \infty. \end{aligned} \tag{22}$$

Next, [61] led to determining the stability of the dual solutions,

$$f(\eta, \tau) = f_0(\eta) + e^{-\gamma \tau} F(\eta), \quad \theta(\eta, \tau) = \theta_0(\eta) + e^{-\gamma \tau} G(\eta), \tag{23}$$

where  $\gamma$  denotes the unknown eigenvalue while  $F(\eta)$  and  $G(\eta)$  are small in comparison to  $f_0(\eta)$  and  $\theta_0(\eta)$ . Then, by substituting Eq. (23) into Eqs. (20) – (21), the following linear eigenvalue problems are obtained:

$$3 \frac{\mu_{hnf}}{\mu_f} F''' + 2 \frac{\rho_{hnf}}{\rho_f} (f_0 F'' + f''_0 F - f'_0 F') + \frac{\rho_{hnf}}{\rho_f} \gamma F' - 3 \frac{\sigma_{hnf}}{\sigma_f} M F' = 0, \tag{24}$$

$$\frac{3}{Pr} \left( \frac{k_{hnf}}{k_f} + \frac{4}{3} R \right) G'' + 2 \frac{(\rho C_p)_{hnf}}{(\rho C_p)_f} [f_0 G' + \theta'_0 F] + \frac{(\rho C_p)_{hnf}}{(\rho C_p)_f} \gamma G = 0, \tag{25}$$

subject to

$$\begin{aligned} F(0) = 0, \quad F'(0) = 0, \quad G(0) = 0, \\ F'(\eta) = 0, \quad G(\eta) = 0 \quad \text{as} \quad \eta \rightarrow \infty. \end{aligned} \tag{26}$$

The smallest eigenvalue ( $\gamma$ ) is used to determine the steady flow solutions' stability  $F(\eta)$  and  $G(\eta)$ . In the study of [65], proposed that a suitable boundary condition be relaxed on either  $F_0$  or  $G_0$  in order to obtain a wider  $\gamma$  range. Thus, the requirement  $F_0' \rightarrow 0$  is relaxed when  $\eta \rightarrow \infty$ , and given a fixed value of  $\gamma$ , the Eqs. (24)–(26) have been solved using the new boundary conditions  $F_0''(0) = 1$ . Notably, the solutions to Eqs. (24)–(26) may provide an infinite number of eigenvalues  $\gamma_1 < \gamma_2 < \gamma_3 < \dots$ , where  $\gamma_1$  is the smallest eigenvalue parameter. Additionally, a positive  $\gamma_1$  indicates an initial decline in disturbances and a stable flow, whereas a negative  $\gamma_1$  indicates an initial increase in disturbances and an unstable flow.

### 4. Results and discussion

The mathematical models of ordinary differential equations (ODE) Eqs. (9)–(10) are numerically solved using the MATLAB software package bvp4c in conjunction with the boundary conditions in Eq. (11). Numerous researchers have commonly employed this technique to address the issues on the boundary layer. These results are generated by establishing an initial guess at a mesh point and increasing the step size till its requisite precision is obtained. The stretching/shrinking parameter  $c$ , the volume percentage of  $Al_2O_3$  ( $\phi_1$ ) and  $Cu$  ( $\phi_2$ ) nanoparticles, the Prandtl number ( $Pr$ ), the magnetic parameter ( $M$ ), the radiation parameter ( $R$ ), and the suction parameter ( $s$ ) are all employed. Following that, the appropriate initial guess and the thickness of the boundary layer must be computed by relying on the parameters reading. The Prandtl number for water is 6.2 meanwhile, the nanoparticle volume fraction of  $Al_2O_3$  is 0.1, which remains constant throughout this problem to determine the numerical answer. The acquired results were tabulated as numerical solutions and graphics. The numerical results are corroborated by comparison to earlier studies, which are listed in Tables 3 and 4, with the skin friction coefficient and local Nusselt number values sequentially. It is noted that the current findings are highly compatible with those of [31,66,67]. The current numerical results indicate that a dual solution exists for specified parameter values of  $M$ ,  $R$ ,  $s$  and  $\phi_2$ .

Table 5 illustrates the influence of physical parameters  $M$  and  $R$  on heat transfer between water, nanofluid, and hybrid nanofluid across a nonlinearly expanding surface with  $s = 2.2$  and  $Pr = 6.2$ . Nanofluids transmit heat more rapidly than hybrid nanofluids. Additionally, water's heat transfer rate is greater than nanofluids and hybrid nanofluids. However, the parameters  $M$  and  $R$  have a major effect on all three fluids, as their values accelerate the rate of heat transfer.

The figures depict numerical readings for the skin friction coefficient ( $Re_x^{1/2} C_f$ ), the local Nusselt number ( $Re_x^{-1/2} Nu_x$ ), the velocity profile ( $f'(\eta)$ ), and the temperature profile ( $\theta(\eta)$ ) considering various values of influencing parameters. The critical values,  $c_c$ , represent the intersection of the first and second solution. As seen in Fig. 1, the skin friction coefficient evolves as  $M$  approaches 0, 0.05, and 0.1 in proportion to  $c$ . Increment in parameter  $M$  results in decreasing value of skin friction coefficient for first solution and second solutions as  $c > -1$ . The behaviour of the local Nusselt number concerning parameter  $c$  as parameter  $M$  varies is depicted in Fig. 2. The first solution for the local Nusselt number exhibits an increasing value as the parameter of  $M$  increases. However, when  $M$  increases, the second solution follows the opposite trend for  $c > -1$ .

Figs. 3 and 4 show the effect of various  $M$  parameters on the velocity and temperature profiles versus parameter  $c$ . According to the first solution of the figures, raising in  $M$  increases the hybrid nanofluid velocity and temperature. However, reverse trends in velocity and temperature of the hybrid nanofluid for the second solution. Additionally, the graph in Fig. 2 demonstrates that as the parameter of  $M$  raised, the thermal boundary layer thickens in both solutions. The resistance of Lorentz force cause by magnetic field, assists fluid velocity, improves fluid temperature, and accelerate the thermal boundary layer separation. Thus, enhancing the hybrid nanofluid's heat transfer rate.

Figs. 5 and 6 exemplify the impact of parameter  $R$  on local Nusselt number and temperature profiles. Several chosen variants of parameter  $R$  are 1, 2, and 3. As parameter  $R$  increases, the local Nusselt number drops for the first solution while it overturns in second

**Table 3**

The comparison of skin friction coefficient,  $f''(0)$  for a base fluid ( $\phi_1 = \phi_2 = 0$ ) with various values of  $s$  where  $R = 0$  and  $c = 1$ .

$s$	Waini et al. [31]	Ferdows et al. [66]	Rashidi et al. [67]	Present result
0.75	-0.984439	-0.984439	-0.9844401	-0.984439
0.5	-0.873643	-0.873643	-0.8736447	-0.873643
0	-0.677648	-0.677648	-0.6776563	-0.677648
-0.5	-0.518869	-0.518869	-0.5188901	-0.518869
-0.75	-0.453523	-0.453523	-0.4535499	-0.453523

**Table 4**

The comparison of local Nusselt number,  $-\theta'(0)$  using base fluid ( $\phi_1 = \phi_2 = 0$ ) with various values of  $s$  and  $R$  where  $c = 1$  and  $Pr = 2$ .

$s$	$R$	Waini et al. [31]	Ferdows et al. [66]	Ferdows et al. [66]	Present Result
0.5	1	0.6322	0.632199	0.6322186	0.6322
	0	1.230792	1.230952	1.2307912	1.230792
0	1	0.443323	0.443323	0.4434039	0.443323
	0	0.764357	0.764374	0.7643525	0.764357
-0.5	1	0.287485	0.287483	0.2877089	0.287485
	0	0.3991	0.398951	0.3990842	0.3991

**Table 5**

The rate of heat transfer ( $Re_x^{-1/2}Nu_x$ ) comparison between water, nanofluid, and hybrid nanofluid.

$M$	$R$	Water ( $\phi_1 = \phi_2 = 0$ )	Nanofluid ( $\phi_1 = 0.1, \phi_2 = 0$ )	Hybrid Nanofluid ( $\phi_1 = 0.1, \phi_2 = 0.1$ )
0	1	9.769941	9.575848	9.463926
0.05		9.772354	9.578054	9.465512
0.1		9.774838	9.580311	9.46712
0	2	9.991361	9.777768	9.622206
0.05		9.995607	9.78137	9.624543
0.1		9.999988	9.785059	9.626913
0	3	10.157448	9.930463	9.74026
0.05		10.163436	9.935367	9.74326
0.1		10.169624	9.940397	9.746305

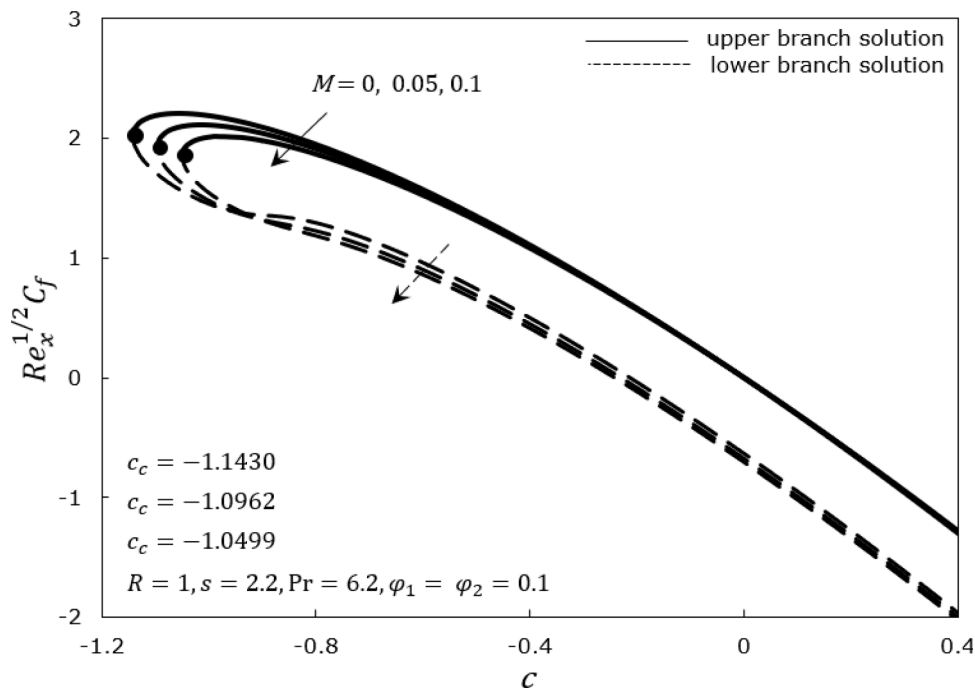


**Fig. 1.** The variation of  $Re_x^{-1/2}C_f$  as parameter  $M$  varies.

solution as shown in Fig. 5. Additionally, the  $c_c$  for the local Nusselt number graph are found to be almost comparable with values of  $-1.0499, -1.0498,$  and  $-1.0499$ . Meanwhile, Fig. 6 illustrates an increase value of first and second solutions when parameter  $R$  grows. Thus, parameter  $R$  leads to the increment of hybrid nanofluid temperature. The radiation parameter  $R$ , as defined by [31], is the inverse of the Stark number that quantifies the proportional contribution of thermal radiation in conducting heat transport. More significant amounts of  $R$  suggest that thermal radiation outperforms conduction. Consequently, a greater rate of  $R$  indicates that more radiative heat transfer happens further into the flow field, leading to an increase in temperature.

Following that, Figs. 7 and 8 demonstrate velocity and temperature profiles as  $s$  fluctuates. The chosen values of  $s$  are 2.2, 2.3, and 2.4. Figures depict the additional of  $s$  parameter, declining the velocity and temperature gradient in first solutions. Meanwhile, the

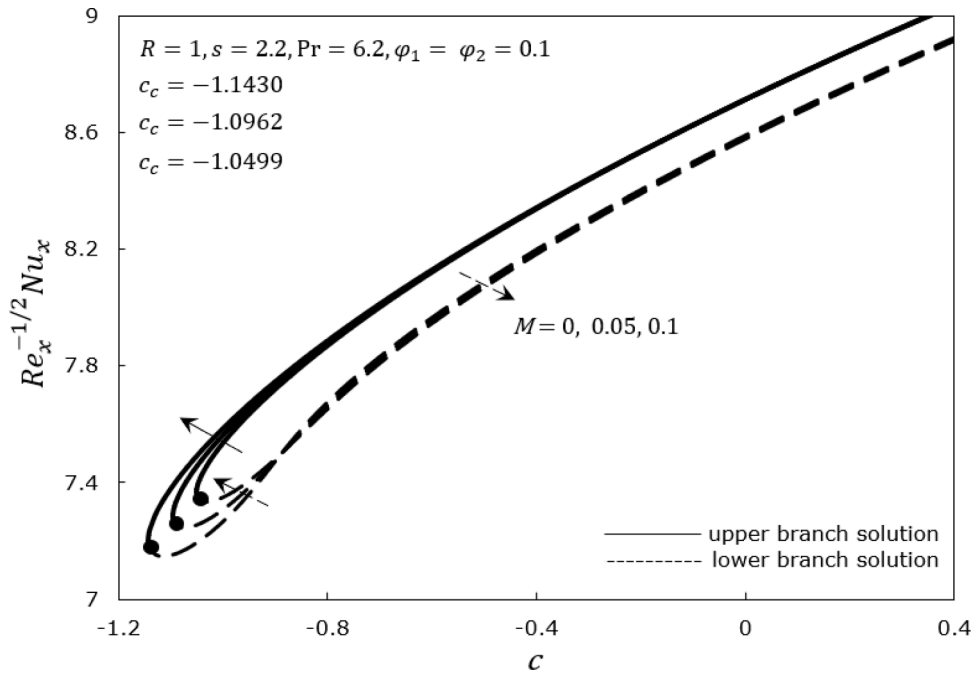


Fig. 2. The variation of  $Re_x^{-1/2} Nu_x$  as parameter  $M$  varies.

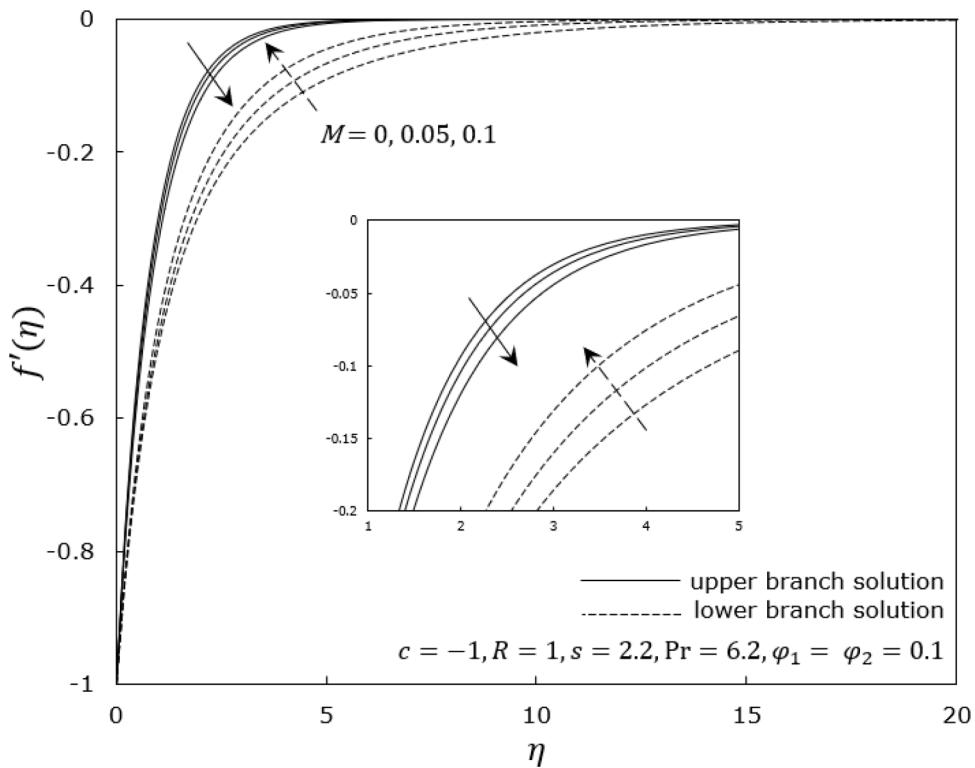


Fig. 3. The variation of  $f'(\eta)$  for parameter  $M$  varies.

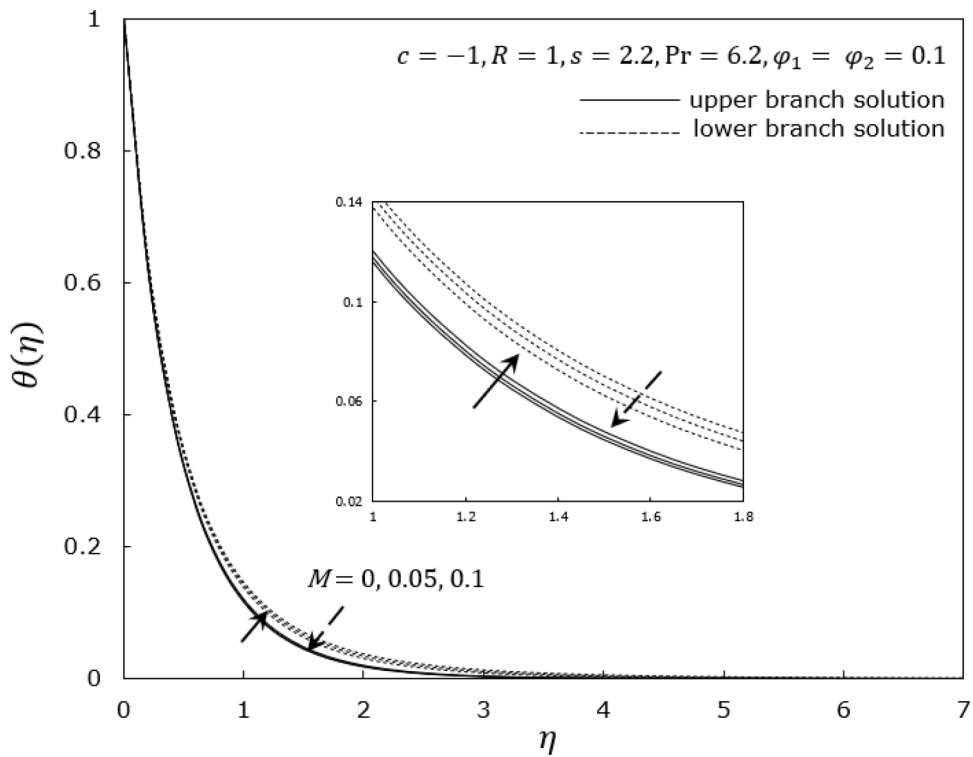


Fig. 4. The variation of  $\theta(\eta)$  for parameter  $M$  varies.

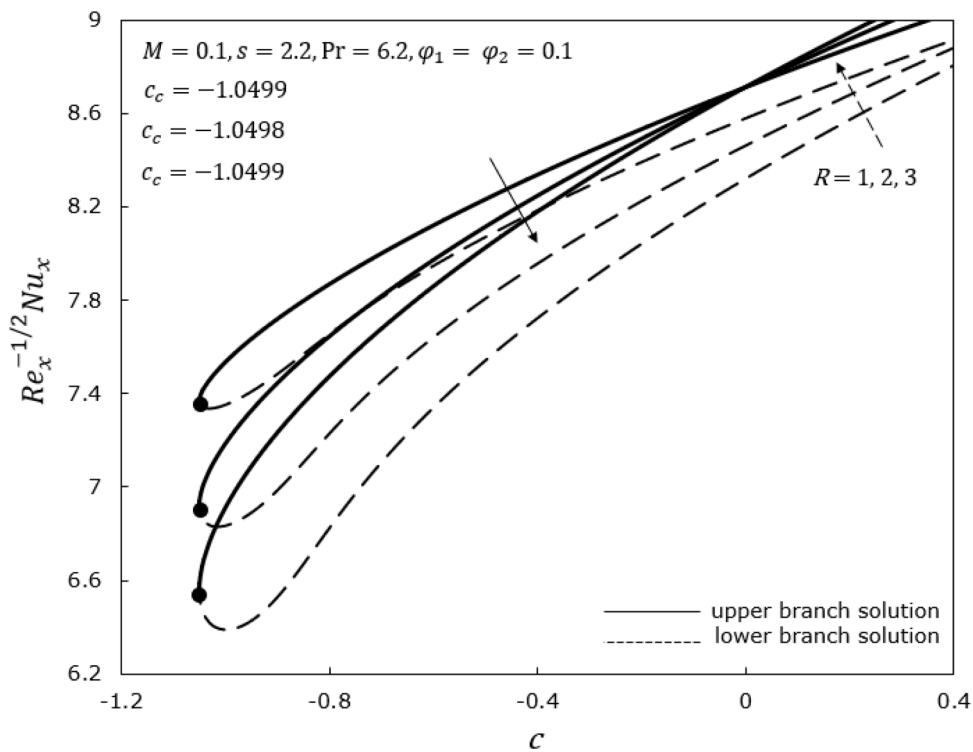


Fig. 5. The variation of  $Re_x^{-1/2} Nu_x$  for parameter  $R$  varies.

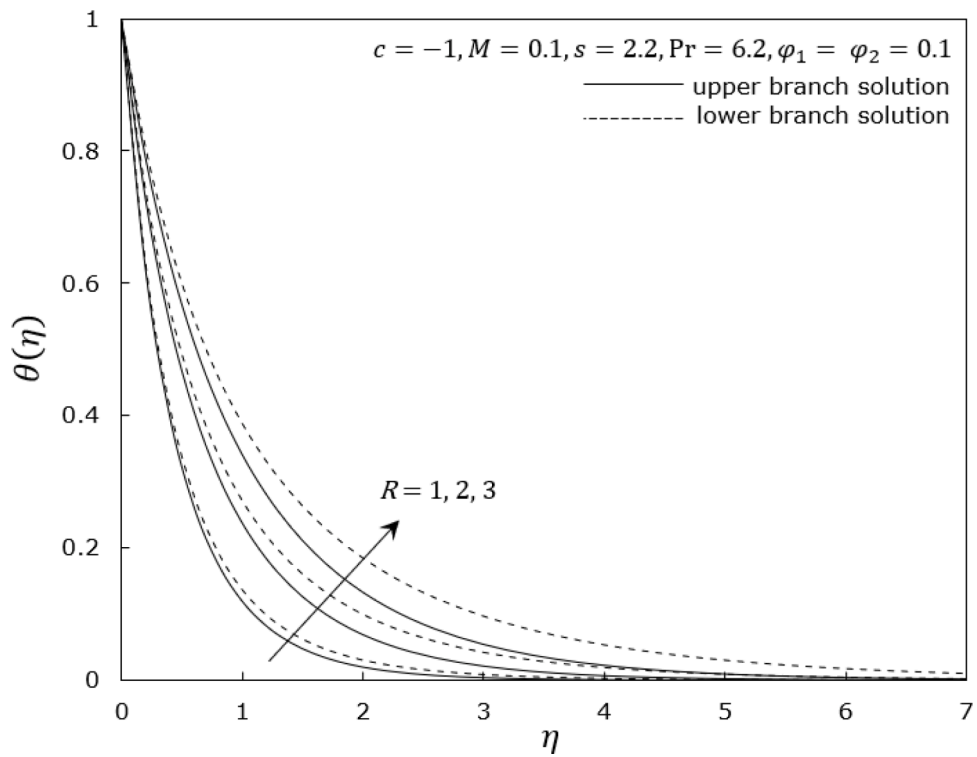


Fig. 6. The variation of  $\theta(\eta)$  for parameter  $R$  varies.

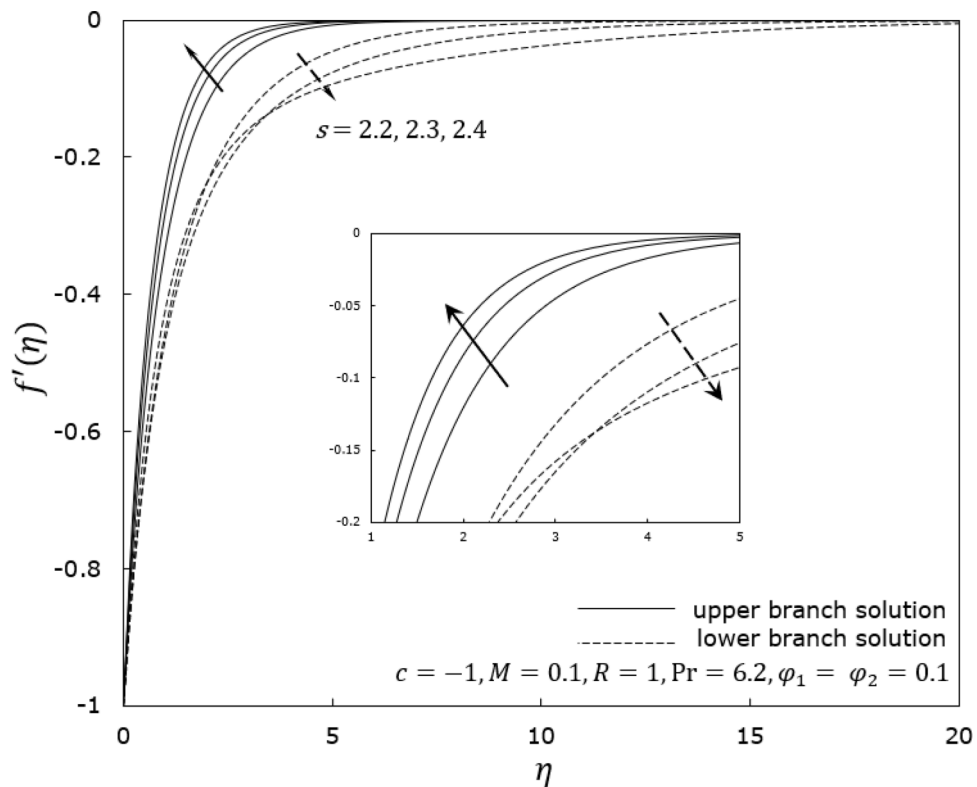


Fig. 7. The variation of  $f'(\eta)$  as parameter  $s$  varies.

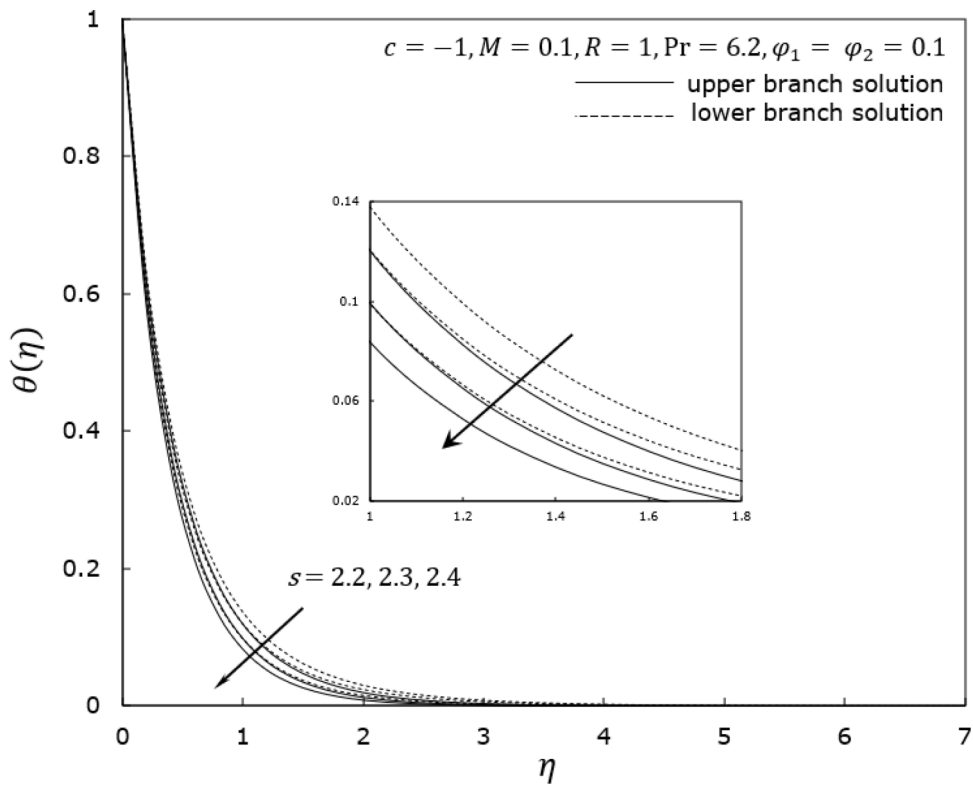


Fig. 8. The variation for  $\theta(\eta)$  as parameter  $s$  varies.

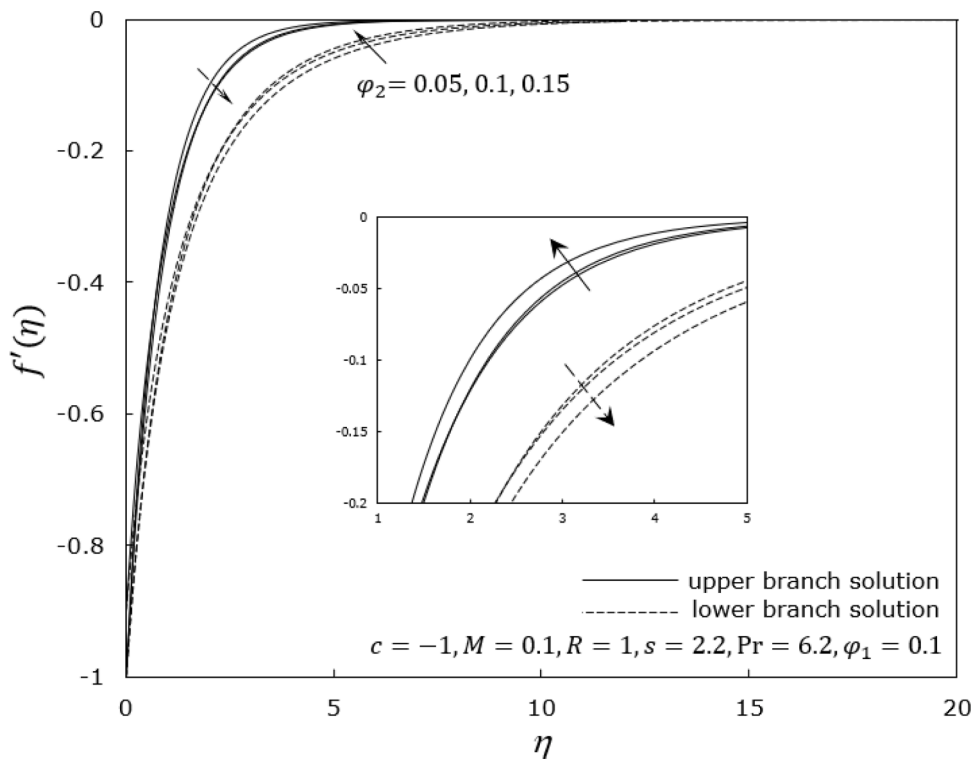


Fig. 9. The variation of  $f'(\eta)$  as parameter  $\phi_2$  varies.

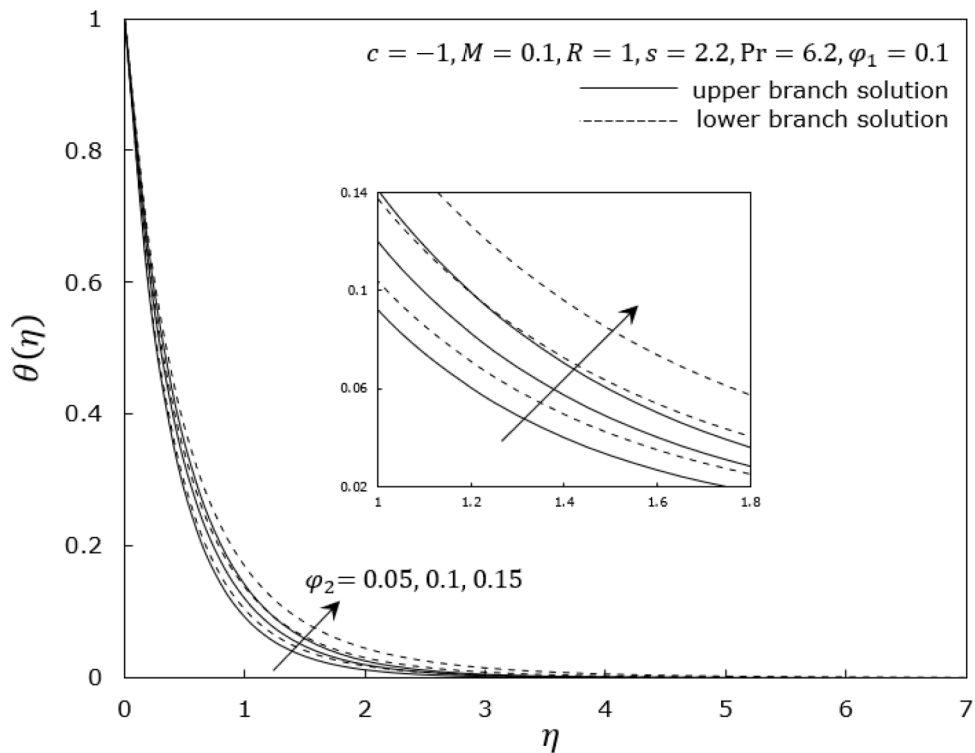


Fig. 10. The variation of  $\theta(\eta)$  as parameter  $\phi_2$  varies.

Table 6

The smallest eigenvalues as  $R = 1, s = 2.2, \phi_1 = \phi_2 = 0.1$ .

$M$	$c$	First solution( $\gamma_1$ )	Second solution ( $\gamma_1$ )
0	-0.8	4.7904	-0.3029
	-1.14	3.9919	-0.0874
	-1.143	2.2098	-0.0001
0.05	-0.1	4.1056	-0.2578
	-0.5	3.5866	-0.2109
	-1.04	1.4019	-0.1792
0.1	-0.5	3.6503	-0.1075
	-0.8	3.1802	-0.1022
	-1	1.5148	-0.012

second solution shows increasing in velocity gradient and decreasing in temperature gradient. Thus, the existence of  $s$  parameter in hybrid nanofluid flow leads to the decreases fluid flow and convective heat transfer rates. In Figs. 9 and 10, the velocity and temperature profiles are plotted against the fluctuation in the nanoparticle volume fraction of copper ( $\phi_2$ ), which is 0.05, 0.1, and 0.15, respectively. As  $\phi_2$  increases, the velocity gradient decreases for both solutions, as illustrated in Fig. 9. Meanwhile, the temperature gradient increases as  $\phi_2$  incline for both solutions in Fig. 10. Thus, raising  $\phi_2$  decreases the velocity of hybrid nanofluid while enhancing its temperature.

Finally, stability analysis is executed on Eqs. (24)–(26) in the MATLAB bvp4c software to calculate the smallest eigenvalues ( $\gamma_1$ ) in the range  $c > c_c$ , where  $c_c$  is the critical value of  $c$ . It is critical to refer to the sign of  $\gamma_1$  while establishing the stability of solutions. In dual solution, the result of smallest eigenvalues is displayed in Table 6, with the first and second solutions denoted by  $\gamma_1 > 0$  and  $\gamma_1 < 0$ , respectively. The first solution found to be stable solution because the value of  $\gamma_1$  is positive whereas the second solution reveals an unstable solution because the value of  $\gamma_1$  is negative. A stable solution displays the solution’s stabilising property in response to a specific disturbance, whereas an unstable solution demonstrates the extension of the disturbance, resulting in flow separation.

### 5. Conclusions

The study investigates the magnetohydrodynamic (MHD) flow and heat transport of a hybrid nanofluid beneath a nonlinearly stretching/shrinking surface using the bvp4c tool in MATLAB. The numerical data empowers the following conclusions:

- It is discovered that if the stretching/shrinking parameter ( $c$ ) is varied, a dual solution and unique solutions exist for a specific range.
- Water has superior heat transfer performance compared to nanofluids and hybrid nanofluids.
- Increases in the magnetic parameter ( $M$ ), increase the hybrid nanofluid velocity, temperature and convective heat transfer rate whereas decrease the skin friction coefficient.
- The increment of parameter  $R$  raises the hybrid nanofluid temperature and diminish the heat transfer rate.
- The existence of suction parameter ( $s$ ) in hybrid nanofluid flow leads to the decreases fluid flow and convective heat transfer rates.
- Rises in copper volume fraction nanoparticles ( $\phi_2$ ), result in an increment of hybrid nanofluid temperature and reduction of its velocity.
- Stability analysis shows that solution of the first solution is steady while the second solution is unsteady.
- Additional studies on MHD and thermal radiation should be conducted using an array of aspects to optimize the heat transfer rate on hybrid nanofluids for industrial applications.

### Declaration of Competing Interest

The authors declare that they have no known competing financial interests or personal relationships that could have appeared to influence the work reported in this paper.

### Acknowledgement

CRG provided funding for this research via the Universiti Pertahanan Nasional Malaysia under the project code CRG/UPNM/2019/ST/04 and Universiti Teknikal Malaysia Melaka are acknowledged.

### References

- [1] S. Masood, M. Farooq, Influence of thermal stratification and thermal radiation on graphene oxide-Ag/H<sub>2</sub>O hybrid nanofluid, *J. Therm. Anal. Calorim.* 143 (2) (2020) 1361–1370, <https://doi.org/10.1007/s10973-020-10227-7>.
- [2] S.K. Soid, A. Ishak, I. Pop, Boundary layer flow past a continuously moving thin needle in a nanofluid, *Appl. Therm. Eng.* 114 (2017) 58–64, <https://doi.org/10.1016/j.applthermaleng.2016.11.165>.
- [3] J.A. Khan, M. Mustafa, T. Hayat, M. Turkyilmazoglu, A. Alsaedi, Numerical study of nanofluid flow and heat transfer over a rotating disk using Buongiorno's model, *Int. J. Numer. Methods Heat Fluid Flow* 27 (1) (2017) 221–234, <https://doi.org/10.1108/HFF-08-2015-0328>.
- [4] W. Ibrahim, Magnetohydrodynamic (MHD) boundary layer stagnation point flow and heat transfer of a nanofluid past a stretching sheet with melting, *Propuls. Power Res.* 6 (3) (2017) 214–222, <https://doi.org/10.1016/j.jprr.2017.07.002>.
- [5] W. Ibrahim, A. Tulu, Magnetohydrodynamic (MHD) boundary layer flow past a wedge with heat transfer and viscous effects of nanofluid embedded in porous media, *Math. Probl. Eng.* 2019 (2019) 1–12, <https://doi.org/10.1155/2019/4507852>.
- [6] T. Hayat, S. Qayyum, A. Alsaedi, A. Shafiq, Inclined magnetic field and heat source/sink aspects in flow of nanofluid with nonlinear thermal radiation, *Int. J. Heat Mass Transf.* 103 (2016) 99–107, <https://doi.org/10.1016/j.ijheatmasstransfer.2016.06.055>.
- [7] K. Ramesh, S.U. Khan, M. Jameel, M.I. Khan, Y.-M. Chu, S. Kadry, Bioconvection assessment in Maxwell nanofluid configured by a Riga surface with nonlinear thermal radiation and activation energy, *Surf. Interfaces* 21 (2020), <https://doi.org/10.1016/j.surfin.2020.100749>.
- [8] K. Gangadhar, T. Kannan, K. DasaradhaRamaiah, G. Sakthivel, Boundary layer flow of nanofluids to analyse the heat absorption/generation over a stretching sheet with variable suction/injection in the presence of viscous dissipation, *Int. J. Ambient Energy* 41 (9) (2018) 969–980, <https://doi.org/10.1080/01430750.2018.1501738>.
- [9] M.R. Eid, Chemical reaction effect on MHD boundary-layer flow of two-phase nanofluid model over an exponentially stretching sheet with a heat generation, *J. Mol. Liq.* 220 (2016) 718–725, <https://doi.org/10.1016/j.molliq.2016.05.005>.
- [10] Y.-M. Chu, S. Aziz, M.I. Khan, S.U. Khan, M. Nazeer, I. Ahmad, I. Tlili, Nonlinear radiative bioconvection flow of Maxwell nanofluid configured by bidirectional oscillatory moving surface with heat generation phenomenon, *Phys. Scr.* 95 (10) (2020), <https://doi.org/10.1088/1402-4896/abb7a9>.
- [11] M.U. Sajid, H.M. Ali, Thermal conductivity of hybrid nanofluids: a critical review, *Int. J. Heat Mass Transf.* 126 (2018) 211–234, <https://doi.org/10.1016/j.ijheatmasstransfer.2018.05.021>.
- [12] A. Jamaludin, K. Naganthran, R. Nazar, I. Pop, MHD mixed convection stagnation-point flow of Cu-Al<sub>2</sub>O<sub>3</sub>/water hybrid nanofluid over a permeable stretching/shrinking surface with heat source/sink, *Eur. J. Mech. B. Fluids* 84 (2020) 71–80, <https://doi.org/10.1016/j.euromechflu.2020.05.017>.
- [13] S. Dinarvand, M. Nademi Rostami, Mixed convection of a cu-ag/water hybrid nanofluid along a vertical porous cylinder via modified Tiwari–Das model, *J. Theoret. Appl. Mech.* 49 (2) (2019), <https://doi.org/10.7546/jtam.49.19.02.05>.
- [14] A. Jamaludin, R. Nazar, K. Naganthran, I. Pop, Mixed convection hybrid nanofluid flow over an exponentially accelerating surface in a porous media, *Neural Comput. Appl.* 33 (22) (2021) 15719–15729, <https://doi.org/10.1007/s00521-021-06191-4>.
- [15] N.S. Khashi'ie, N.M. Arifin, I. Pop, N.S. Wahid, Flow and heat transfer of hybrid nanofluid over a permeable shrinking cylinder with Joule heating: a comparative analysis, *Alex. Eng. J.* 59 (3) (2020) 1787–1798, <https://doi.org/10.1016/j.aej.2020.04.048>.
- [16] M.N. Rostami, S. Dinarvand, I. Pop, Dual solutions for mixed convective stagnation-point flow of an aqueous silica–alumina hybrid nanofluid, *Chin. J. Phys.* 56 (5) (2018) 2465–2478, <https://doi.org/10.1016/j.cjph.2018.06.013>.
- [17] M. Ghalambaz, N.C. Roşca, A.V. Roşca, I. Pop, Mixed convection and stability analysis of stagnation-point boundary layer flow and heat transfer of hybrid nanofluids over a vertical plate, *Int. J. Numer. Methods Heat Fluid Flow* 30 (7) (2019) 3737–3754, <https://doi.org/10.1108/HFF-08-2019-0661>.
- [18] N.S. Khashi'ie, N.M. Arifin, I. Pop, R. Nazar, E.H. Hafidzuddin, A new similarity solution with stability analysis for the three-dimensional boundary layer of hybrid nanofluids, *Int. J. Numer. Methods Heat Fluid Flow* 31 (3) (2020) 809–828, <https://doi.org/10.1108/hff-04-2020-0200>.
- [19] N.A.L. Aladdin, N. Bachok, Boundary layer flow and heat transfer of Al<sub>2</sub>O<sub>3</sub>-TiO<sub>2</sub>/water hybrid nanofluid over a permeable moving plate, *Symmetry (Basel)* 12 (7) (2020), <https://doi.org/10.3390/sym12071064>.
- [20] M. Ijaz Khan, S. Qayyum, F. Shah, R. Naveen Kumar, R.J. Punith Gowda, B.C. Prasannakumara, Y.-M. Chu, S. Kadry, Marangoni convective flow of hybrid nanofluid (MnZnFe<sub>2</sub>O<sub>4</sub>-NiZnFe<sub>2</sub>O<sub>4</sub>-H<sub>2</sub>O) with Darcy Forchheimer medium, *Ain Shams Eng. J.* 12 (4) (2021) 3931–3938, <https://doi.org/10.1016/j.asej.2021.01.028>.
- [21] S.A. Devi, S.S.U. Devi, Numerical investigation of hydromagnetic hybrid Cu–Al<sub>2</sub>O<sub>3</sub>/water nanofluid flow over a permeable stretching sheet with suction, *Int. J. Nonlinear Sci. Numer. Simul.* 17 (5) (2016) 249–257, <https://doi.org/10.1515/ijnsns-2016-0037>.
- [22] B. Ramadevi, K. Anantha Kumar, V. Sugunamma, J.V. Ramana Reddy, N. Sandeep, Magnetohydrodynamic mixed convective flow of micropolar fluid past a stretching surface using modified Fourier's heat flux model, *J. Therm. Anal. Calorim.* 139 (2) (2019) 1379–1393, <https://doi.org/10.1007/s10973-019-08477-1>.

- [23] A.C. Venkata Ramudu, K. Anantha Kumar, V. Sugunamma, N. Sandeep, Impact of Soret and Dufour on MHD Casson fluid flow past a stretching surface with convective–diffusive conditions, *J. Therm. Anal. Calorim.* 147 (3) (2021) 2653–2663, <https://doi.org/10.1007/s10973-021-10569-w>.
- [24] A.K. Kempnangari, R.R. Buruju, S. Naramgari, S. Vangala, Effect of Joule heating on MHD non-Newtonian fluid flow past an exponentially stretching curved surface, *Heat Transf.* 49 (6) (2020) 3575–3592, <https://doi.org/10.1002/hjt.21789>.
- [25] M.I. Khan, F. Alzahrani, Entropy-optimized dissipative flow of Carreau–Yasuda fluid with radiative heat flux and chemical reaction, *Euro. Phys. J. Plus* 135 (6) (2020), <https://doi.org/10.1140/epjp/s13360-020-00532-3>.
- [26] N. Ahmed, F. Saba, U. Khan, S.T. Mohyud-Din, E.-S.M. Sherif, I. Khan, Nonlinear thermal radiation and chemical reaction effects on a (Cu–CuO)/NaAlg hybrid nanofluid flow past a stretching curved surface, *Processes* 7 (12) (2019), <https://doi.org/10.3390/pr7120962>.
- [27] Y.-M. Chu, B.M. Shankaralingappa, B.J. Gireesha, F. Alzahrani, M.I. Khan, S.U. Khan, Combined impact of Cattaneo-Christov double diffusion and radiative heat flux on bio-convective flow of Maxwell liquid configured by a stretched nano-material surface, *Appl. Math. Comput.* 419 (2022), <https://doi.org/10.1016/j.amc.2021.126883>.
- [28] K. Naganthran, R. Nazar, I. Pop, Dual solutions of three-dimensional flow and heat transfer over a non-linearly stretching/shrinking sheet, *Indian J. Phys.* 92 (5) (2018) 637–645, <https://doi.org/10.1007/s12648-017-1144-6>.
- [29] A. Malvandi, F. Hedayati, D. Ganji, Nanofluid flow on the stagnation point of a permeable non-linearly stretching/shrinking sheet, *Alex. Eng. J.* 57 (4) (2018) 2199–2208, <https://doi.org/10.1016/j.aej.2017.08.010>.
- [30] M.E.H. Hafidzuddin, K. Naganthran, R. Nazar, N.M. Arifin, Effect of suction on the MHD fluid flow past a non-linearly stretching/shrinking sheet: dual solutions, *J. Phys. Conf. Ser.* (2019), 012027, <https://doi.org/10.1088/1742-6596/1366/1/012027>.
- [31] I. Waini, A. Ishak, I. Pop, Hybrid nanofluid flow and heat transfer over a nonlinear permeable stretching/shrinking surface, *Int. J. Numer. Methods Heat Fluid Flow* 29 (9) (2019) 3110–3127, <https://doi.org/10.1108/HFF-07-2019-0557>.
- [32] N.C. Roşca, A.V. Roşca, I. Pop, Axisymmetric flow of hybrid nanofluid due to a permeable non-linearly stretching/shrinking sheet with radiation effect, *Int. J. Numer. Methods Heat Fluid Flow* (2020), <https://doi.org/10.1108/HFF-09-2020-0574>.
- [33] I. Waini, A. Ishak, I. Pop, Flow and heat transfer along a permeable stretching/shrinking curved surface in a hybrid nanofluid, *Phys. Scr.* 94 (10) (2019), <https://doi.org/10.1088/1402-4896/ab0fd5>.
- [34] I. Waini, A. Ishak, I. Pop, Transpiration effects on hybrid nanofluid flow and heat transfer over a stretching/shrinking sheet with uniform shear flow, *Alex. Eng. J.* 59 (1) (2020) 91–99, <https://doi.org/10.1016/j.aej.2019.12.010>.
- [35] K. Anantha Kumar, J.V. Ramana Reddy, V. Sugunamma, N. Sandeep, Magneto-hydrodynamic Cattaneo-Christov flow past a cone and a wedge with variable heat source/sink, *Alex. Eng. J.* 57 (1) (2018) 435–443, <https://doi.org/10.1016/j.aej.2016.11.013>.
- [36] K. Anantha Kumar, N. Sandeep, V. Sugunamma, L.L. Animasaun, Effect of irregular heat source/sink on the radiative thin film flow of MHD hybrid ferrofluid, *J. Therm. Anal. Calorim.* 139 (3) (2019) 2145–2153, <https://doi.org/10.1007/s10973-019-08628-4>.
- [37] N.A. Zainal, R. Nazar, K. Naganthran, I. Pop, MHD flow and heat transfer of hybrid nanofluid over a permeable moving surface in the presence of thermal radiation, *Int. J. Numer. Methods Heat Fluid Flow* 31 (3) (2020) 858–879, <https://doi.org/10.1108/HFF-03-2020-0126>.
- [38] U. Yashkun, K. Zaimi, N.A. Abu Bakar, A. Ishak, I. Pop, MHD hybrid nanofluid flow over a permeable stretching/shrinking sheet with thermal radiation effect, *Int. J. Numer. Methods Heat Fluid Flow* 31 (3) (2020) 1014–1031, <https://doi.org/10.1108/HFF-02-2020-0083>.
- [39] E.H. Aly, A. Ebaid, MHD Marangoni boundary layer problem for hybrid nanofluids with thermal radiation, *Int. J. Numer. Methods Heat Fluid Flow* 31 (3) (2020) 897–913, <https://doi.org/10.1108/hff-05-2020-0245>.
- [40] K. Anantha Kumar, V. Sugunamma, N. Sandeep, Influence of viscous dissipation on MHD flow of micropolar fluid over a slendering stretching surface with modified heat flux model, *J. Therm. Anal. Calorim.* 139 (6) (2020) 3661–3674, <https://doi.org/10.1007/s10973-019-08694-8>.
- [41] N.S. Khashi'ie, N.M. Arifin, R. Nazar, E.H. Hafidzuddin, N. Wahi, I. Pop, Magneto-hydrodynamics (MHD) axisymmetric flow and heat transfer of a hybrid nanofluid past a radially permeable stretching/shrinking sheet with Joule heating, *Chin. J. Phys.* 64 (2020) 251–263, <https://doi.org/10.1016/j.cjph.2019.11.008>.
- [42] N.A. Zainal, R. Nazar, K. Naganthran, I. Pop, MHD mixed convection stagnation point flow of a hybrid nanofluid past a vertical flat plate with convective boundary condition, *Chin. J. Phys.* 66 (2020) 630–644, <https://doi.org/10.1016/j.cjph.2020.03.022>.
- [43] A. Kumar, V. Sugunamma, N. Sandeep, Impact of non-linear radiation on MHD non-aligned stagnation point flow of micropolar fluid over a convective surface, *J. NonEquilib. Thermodyn.* 43 (4) (2018) 327–345, <https://doi.org/10.1515/jnet-2018-0022>.
- [44] M. Nazeer, F. Hussain, M.I. Khan, E.R. El-Zahar, Y.M. Chu, M.Y. Malik, Theoretical study of MHD electro-osmotically flow of third-grade fluid in micro channel, *Appl. Math. Comput.* 420 (2022), <https://doi.org/10.1016/j.amc.2021.126868>.
- [45] M. Turkyilmazoglu, Flow and heat over a rotating disk subject to a uniform horizontal magnetic field, *Z. Naturforsch. A* 77 (4) (2022) 329–337, <https://doi.org/10.1515/zna-2021-0350>.
- [46] T.H. Zhao, M.I. Khan, Y.M. Chu, Artificial neural networking (ANN) analysis for heat and entropy generation in flow of non-Newtonian fluid between two rotating disks, *Math. Methods Appl. Sci.* (2021), <https://doi.org/10.1002/mma.7310>.
- [47] K. Anantha Kumar, V. Sugunamma, N. Sandeep, Effect of thermal radiation on MHD Casson fluid flow over an exponentially stretching curved sheet, *J. Therm. Anal. Calorim.* 140 (5) (2019) 2377–2385, <https://doi.org/10.1007/s10973-019-08977-0>.
- [48] K.A. Kumar, V. Sugunamma, N. Sandeep, A non-Fourier heat flux model for magnetohydrodynamic micropolar liquid flow across a coagulated sheet, *Heat Transf.-Asian Res.* 48 (7) (2019) 2819–2843, <https://doi.org/10.1002/hjt.21518>.
- [49] K.A. Kumar, V. Sugunamma, N. Sandeep, M. Mustafa, Simultaneous solutions for first order and second order slips on micropolar fluid flow across a convective surface in the presence of Lorentz force and variable heat source/sink, *Sci. Rep.* 9 (1) (2019) 1–14, <https://doi.org/10.1038/s41598-019-51242-5>.
- [50] A. Jamaludin, K. Naganthran, R. Nazar, I. Pop, Thermal radiation and MHD effects in the mixed convection flow of Fe<sub>3</sub>O<sub>4</sub>–water ferrofluid towards a nonlinearly moving surface, *Processes* 8 (1) (2020), <https://doi.org/10.3390/pr8010095>.
- [51] I. Thili, M.T. Mustafa, K.A. Kumar, N. Sandeep, Effect of asymmetrical heat rise/fall on the film flow of magnetohydrodynamic hybrid ferrofluid, *Sci. Rep.* 10 (1) (2020) 6677, <https://doi.org/10.1038/s41598-020-63708-y>.
- [52] A.J. Chamkha, A.S. Dogonchi, D.D. Ganji, Magneto-hydrodynamic flow and heat transfer of a hybrid nanofluid in a rotating system among two surfaces in the presence of thermal radiation and Joule heating, *AIP Adv.* 9 (2) (2019), <https://doi.org/10.1063/1.5086247>.
- [53] Y.-M. Chu, M. Nazeer, M.I. Khan, F. Hussain, H. Rafi, S. Qayyum, Z. Abdelmalek, Combined impacts of heat source/sink, radiative heat flux, temperature dependent thermal conductivity on forced convective Rabinowitsch fluid, *Int. Commun. Heat Mass Transf.* 120 (2021), <https://doi.org/10.1016/j.icheatmasstransfer.2020.105011>.
- [54] M.K. Nayak, S. Shaw, M. Ijaz Khan, O.D. Makinde, Y.-M. Chu, S.U. Khan, Interfacial layer and shape effects of modified Hamilton's Crosser model in entropy optimized Darcy-Forchheimer flow, *Alex. Eng. J.* 60 (4) (2021) 4067–4083, <https://doi.org/10.1016/j.aej.2021.02.010>.
- [55] N.S. Khashi'ie, N.M. Arifin, I. Pop, N.S. Wahid, Effect of suction on the stagnation point flow of hybrid nanofluid toward a permeable and vertical Riga plate, *Heat Transf.* 50 (2) (2020) 1895–1910, <https://doi.org/10.1002/hjt.21961>.
- [56] N.S. Anuar, N. Bachok, N.M. Arifin, H. Rosali, Effect of suction/injection on stagnation point flow of hybrid nanofluid over an exponentially shrinking sheet with stability analysis, *CFD Lett.* 11 (12) (2019) 21–33.
- [57] P. Tiam Kapen, C. Gervais Njingang Ketchate, D. Fokwa, G. Tchuen, Linear stability analysis of (Cu-Al<sub>2</sub>O<sub>3</sub>)/water hybrid nanofluid flow in porous media in presence of hydromagnetic, small suction and injection effects, *Alex. Eng. J.* 60 (1) (2021) 1525–1536, <https://doi.org/10.1016/j.aej.2020.11.007>.
- [58] N.A.L. Aladdin, N. Bachok, I. Pop, Cu-Al<sub>2</sub>O<sub>3</sub>/water hybrid nanofluid flow over a permeable moving surface in presence of hydromagnetic and suction effects, *Alex. Eng. J.* 59 (2) (2020) 657–666, <https://doi.org/10.1016/j.aej.2020.01.028>.
- [59] M. Turkyilmazoglu, Radially expanding/contracting and rotating sphere with suction, *Int. J. Numer. Methods Heat Fluid Flow* (2022), <https://doi.org/10.1108/HFF-01-2022-0011>.
- [60] R.K. Tiwari, M.K. Das, Heat transfer augmentation in a two-sided lid-driven differentially heated square cavity utilizing nanofluids, *Int. J. Heat Mass Transf.* 50 (9–10) (2007) 2002–2018, <https://doi.org/10.1016/j.ijheatmasstransfer.2006.09.034>.

- [61] P. Weidman, D. Kubitschek, A. Davis, The effect of transpiration on self-similar boundary layer flow over moving surfaces, *Int. J. Eng. Sci.* 44 (11–12) (2006) 730–737, <https://doi.org/10.1016/j.ijengsci.2006.04.005>.
- [62] R. Cortell, Heat and fluid flow due to non-linearly stretching surfaces, *Appl. Math. Comput.* 217 (19) (2011) 7564–7572, <https://doi.org/10.1016/j.amc.2011.02.029>.
- [63] H.F. Oztop, E. Abu-Nada, Numerical study of natural convection in partially heated rectangular enclosures filled with nanofluids, *Int. J. Heat Fluid Flow* 29 (5) (2008) 1326–1336, <https://doi.org/10.1016/j.ijheatfluidflow.2008.04.009>.
- [64] J. Merkin, On dual solutions occurring in mixed convection in a porous medium, *J. Eng. Math.* 20 (2) (1986) 171–179, <https://doi.org/10.1007/BF00042775>.
- [65] S. Harris, D. Ingham, I. Pop, Mixed convection boundary-layer flow near the stagnation point on a vertical surface in a porous medium: Brinkman model with slip, *Transp. Porous Media* 77 (2) (2009) 267–285, <https://doi.org/10.1007/s11242-008-9309-6>.
- [66] M. Ferdows, M.J. Uddin, A. Afify, Scaling group transformation for MHD boundary layer free convective heat and mass transfer flow past a convectively heated nonlinear radiating stretching sheet, *Int. J. Heat Mass Transf.* 56 (1–2) (2013) 181–187, <https://doi.org/10.1016/j.ijheatmasstransfer.2012.09.020>.
- [67] M.M. Rashidi, B. Rostami, N. Freidoonimehr, S. Abbasbandy, Free convective heat and mass transfer for MHD fluid flow over a permeable vertical stretching sheet in the presence of the radiation and buoyancy effects, *Ain Shams Eng. J.* 5 (3) (2014) 901–912, <https://doi.org/10.1016/j.asej.2014.02.007>.